Submitted to The Astrophysical Journal

The Broadband Afterglow of GRB 980329

S. A. Yost[1], D. A. Frail[1,2], F. A. Harrison[1], R. Sari[3], D. Reichart[1], J. S. Bloom[1], S. R. Kulkarni[1], G. H. Moriarty-Schieven[4] S. G. Djorgovski[1], P. A. Price[1,5], R. W. Goodrich[6], J. E. Larkin[7], F. Walter[1] D. S. Shepherd[2], D. W. Fox[1] G. B. Taylor[2], E. Berger[1], T. J. Galama[1]

ABSTRACT

We present radio observations of the afterglow of the bright γ–ray burst GRB 980329 made between one month and several years after the burst, a re-analysis of previously published submillimeter data, and late-time optical and near-infrared (NIR) observations of the host galaxy. From the absence of a spectral break in the optical/NIR colors of the host galaxy, we exclude the earlier suggestion that GRB 980329 lies at a redshift of $z \gtrsim 5$. We combine our data with the numerous multi-wavelength observations of the early afterglow, fit a comprehensive afterglow model to the entire broadband dataset, and derive fundamental physical parameters of the blast-wave and its host environment. Models for which the ejecta expand isotropically require both a high circumburst density and extreme radiative losses from the shock. No low density model ($n \ll 10$ cm^{-3}) fits the data. A burst with a total energy of $\sim 10^{51}$ erg, with the ejecta narrowly collimated to an opening angle of a few degrees, driven into a surrounding medium with density ~ 20 cm^{-3}, provides a satisfactory fit to the lightcurves over a range of redshifts.

[1]Division of Physics, Mathematics and Astronomy, 105-24, California Institute of Technology, Pasadena, CA 91125

[2]National Radio Astronomy Observatory, P.O. BOX 'O', Socorro, NM 87801

[3]Theoretical Astrophysics 130-33, California Institute of Technology, Pasadena, CA 91125

[4]National Research Council of Canada, Joint Astronomy Centre, 660 N. A'ohoku Place Hilo, HI 96720

[5]Research School of Astronomy and Astrophysics, Mount Stromlo Observatory, via Cotter Rd., Watson Creek 2611, Australia

[6]W. M. Keck Observatory, 65-1120 Mamalahoa Highway, Kamuela, HI 96743

[7]Department of Physics and Astronomy, University of California, Los Angeles, CA 90095

1. Introduction

The discovery of long-lived afterglow emission from gamma-ray bursts (GRBs) has revolutionized the field by enabling redshift determinations and host galaxy identifications. In addition, by interpreting the emission in the theoretical framework of a relativistic shock wave expanding into a circumburst medium, broadband afterglow measurements can constrain the explosion geometry and energetics, as well as the properties of the surrounding medium (Wijers & Galama 1999; Granot, Piran & Sari 1999; Harrison *et al.* 2001; Panaitescu & Kumar 2001b). The hydrodynamic evolution of the blast-wave is strongly influenced by the the total energy in the shock, the geometry of the outflow and the density structure of the medium into which it is expanding. The time-dependence of the radiated emission from the shock depends on the hydrodynamic evolution, as well as on the partition of energy between the radiating electrons and the magnetic field. With data of sufficient quality in conjunction with a theoretical model, broadband measurements of the spectral evolution of the afterglow allow us to deduce fundamental physical parameters of the explosion.

Bright gamma-ray bursts such as GRB 980329 have been targets of extensive broadband followup. GRB 980329 was well-localized in the gamma-rays, and the position quickly refined as a result of the X-ray detection by In't Zand *et al.* (1998). However, initial searches for an optical afterglow were unsuccessful until variable emission was identified at radio wavelengths (Taylor *et al.* 1998). Subsequent observations of the radio position uncovered a faint optical counterpart (Djorgovski *et al.* 1998), as well as a relatively bright near-infrared (NIR) transient (Klose 1998). Because of the delay in the identification of the optical afterglow, the early optical monitoring was somewhat sparse. In spite of the eventual detection of optical and NIR counterparts, no redshift has been determined, due to the faintness of the host emission and its lack of prominent emission lines.

In this paper we present broadband observations of the afterglow of GRB 980329. We monitored the emission at multiple radio frequencies over times extending beyond the first month (early time data were reported by Taylor *et al.* (1998)). In addition, we present late-time optical and NIR observations in the R, I, H and K bands, as well as a re-analysis of submillimeter data reported by Smith *et al.* (1999). We fit the broadband emission to a fireball model, allowing us to derive the physical parameters of the afterglow, and measure the properties of the host galaxy.

2. Observations and Data Reduction

2.1. Optical/NIR Data

Optical and NIR observations were made using the Keck[8] 10-m telescopes on Mauna Kea, Hawaii in the R, I, and K bands. Except for a re-calibration of the K-band points from Larkin *et al.* (1998a,b), all the photometric measurements presented in Table 1 have not been previously published. Deep R- and I-band images were obtained on several epochs using the Low Resolution Imaging Spectrometer (LRIS; Oke *et al.* (1995)), and on one epoch (2001 January) with the Echelle Spectrograph and Imager (ESI; Sheinis *et al.* (2000)). The data consist of multiple CCD exposures with typical durations of 300 s taken in good photometric conditions at an airmass between 1.1 to 1.3. We flat fielded and combined the data following standard practice. For calibration purposes, we used an image of the GRB 980329 field taken at the Palomar 60-inch in January 1999 under photometric conditions. Its photometric zeropoint was determined using four field stars which were in common with Reichart *et al.* (1999).

The K-band images of the GRB 980329 field were taken with the Near Infrared Camera (NIRC; Matthews & Soifer 1994) on the Keck I telescope. We used IRAF to reduce the data, and the DIMSUM package[9] to combine images and subtract sky background. We used observations of Persson *et al.* (1998) standards on each photometric night to calibrate a sequence of stars in the field, against which we performed relative photometry of the afterglow. We estimate that the calibration is accurate to approximately 5%.

We also made use of an H-band observation from the Hubble Space Telescope (*HST*) archive. HST observed GRB 980329 on 1998 October 16 through the F160W filter with NICMOS Camera 2 as part of GO7863 (PI: A. Fruchter). We used the standard NICMOS pipeline developed at STScI with the best available reference and calibration files to process the images. We then shifted and added the exposures to form a final, stacked image. We used the IRAF aperture photometry tools to measure the afterglow flux and the NICMOS photometric calibration published by Stephens *et al.* (2000) to convert this measurement to the standard H-band magnitude.

---

[8]The W. M. Keck Observatory is operated by the California Association for Research in Astronomy, a scientific partnership among California Institute of Technology, the University of California and the National Aeronautics and Space Administration.

[9]http://iraf.noao.edu/iraf/ftp/contrib/dimsumV2/

2.2. Very Large Array (VLA)

Observations were made with the VLA[10] at three frequencies, 8.46 GHz, 4.86 GHz and 1.43 GHz. All observations employed the standard VLA continuum mode, with data being recorded in two adjacent 50 MHz bandpasses. Calibration of the array phase was derived from observations of the nearby calibrators J0653+370 and J0713+438. Calibration of the flux density scale was done using J1331+305 or J0542+498, or by extrapolating past measurements of J0713+438, which was has a very stable flux density. Table 2 contains a log of the observations and a list of the measured flux densities. The VLA data for the first month after the burst were published by Taylor et al. (1998).

2.3. Owens Valley Radio Observatory (OVRO)

A continuum observation with OVRO was made at a central frequency of 99.98 GHz on 1998 Dec 13.42 and 14.40 UT, several months after the burst. The observations totalled approximately 14 hours on source in good 3 mm weather conditions. The total bandwidth was 2 GHz, resulting in an rms of ~ 0.7 mJy. The flux was calibrated using the extragalactic source 3C273, and the phase from the nearby quasar 0552+398.

A further observation was made at a central frequency of 99.5 GHz on 2001 November 26.48 UT, nearly 1400 days after the burst. The observation consisted of a single, 11-hr long track (9 hours on source) taken under excellent 3 mm conditions with four antennas. The total bandwidth was 4 GHz, resulting in an rms of ~ 0.5 mJy. We set the flux density scale using the extragalactic sources 3C84 as well as 3C273, and derived phase calibration from J0646+448.

2.4. James Clark Maxwell Telescope (JCMT)

We re-analyzed archival JCMT[11] observations of this burst taken at frequencies of 650 GHz, 350 GHz and 220 GHz. Details of the observing procedure can be found in Smith *et al.* (1998). The data were reduced using the SCUBA User Reduction Facility (Jenness &

---

[10] The NRAO is a facility of the National Science Foundation operated under cooperative agreement by Associated Universities, Inc. NRAO operates the VLA.

[11] The JCMT is operated by The Joint Astronomy Centre on behalf of the Particle Physics and Astronomy Research Council of the UK, the Netherlands Organization for Scientific Research, and the National Research Council of Canada.

Lightfoot 1998) in the same manner as that for the recent GRB 010222 (Frail *et al.* 2002). Raw signals were flat-fielded to account for the small differences in bolometer response, extinction corrected, and de-spiked to remove anomalous signals above the 3-sigma level. Short time-scale sky variations were also removed using pixels around the edge of the array containing no source emission (Jenness, Lightfoot & Holland 1998). A flux calibration factor was then applied to convert to Jy. Flux calibration factors (FCF) of 240 $\pm$ 15 Jy/V, 197 $\pm$ 13 Jy/V and 384 $\pm$ 82 Jy/V were applied to the 220 GHz, 350 GHz and 660 GHz data, respectively (Coulson 2000). Table 3 contains a log of the observations and a list of the measured flux densities.

3. Afterglow Model

We interpret the data in the framework of the cosmological fireball model (*e.g.*, Piran (1999)), in which an energetic explosion accelerates a small amount of matter to ultrarelativistic velocities. Internal shocks within this flow produce the burst event itself, while the relativistic shock propagating into the surrounding medium produces the afterglow.

In the model, we assume the ultrarelativistic shock transfers a constant fraction of its total energy to the magnetic field (ϵ_B) as well as a constant fraction to shocked, thermalized electrons (ϵ_e). As in strong subrelativistic shocks, the electrons are assumed to be accelerated into a power–law distribution of energies ($P(\gamma_e) \propto \gamma^{-p}$) and they radiate via synchrotron emission under the influence of magnetic fields. This produces a broken power–law spectrum whose peak and spectral breaks evolve in time according to the shock's behaviour (Sari, Piran & Narayan 1998), set by the total energy in the shock, the geometry of the ejecta and the density of matter surrounding it.

The specific model we used to fit the data is outlined in some detail in Harrison *et al.* (2001). It includes the effects of inverse Compton (IC) scattering on the shock evolution and emitted radiation spectrum as prescribed by Sari & Esin (2001). It allows for a conical (jet-like) outflow geometry with half-opening angle θ_{jet} (using the treatment given by Sari, Piran & Halpern (1999)), and for expansion into a medium of constant density n, or a medium with a density gradient, *i.e.*, $n \propto r^{-2}$. The latter density profile would be typical of a medium altered by the wind of a massive star (in this case the GRB progenitor). In addition, we calculate and include radiative corrections to the shock energy. This is a refined method as compared to the adiabatic evolution typically assumed in our previous work (Harrison *et al.* 2001; Berger *et al.* 2001a, 2000). We approximate the radiative evolution by treating the shock at each moment as though it were instantaneously adiabatic, with an energy calculated at that particular time. This is an appropriate treatment as long as losses are moderate, with the change in energy being slow.

In addition to the basic input physics describing the evolution of the fireball outlined above, the broadband model for GRB afterglows incorporates several additional effects resulting from propagation of the radiation between the fireball and the observer. These include interstellar scintillation in the centimeter radio regime, dust extinction in the optical/NIR regime, and a contribution to the emission from the host galaxy of the GRB. These features are evident in the data, and must be included to derive accurate model parameters.

Interstellar scintillation (ISS), due to the turbulent ionized gas of our Galaxy distorting wavefronts propagating to the observer, can be important at radio wavelengths (Goodman 1997; Frail *et al.* 1997). We account for ISS by first estimating the fractional variation in the flux density expected by these distortions (Walker 1998). This uncertainty in the model flux is added in quadrature to the statistical uncertainties in the measured values when estimating χ^2.

Dust within GRB host galaxies (either in the circumburst environment or along the line of sight) is a source of extinction for optical/NIR afterglows (Klose *et al.* 2000; Sokolov *et al.* 2001; Djorgovski *et al.* 2001) which must be accounted for in modeling the optical spectrum. The frequency dependence of the extinction curve is uncertain, since we know little about the ISM properties of the GRB 980329 host galaxy. For GRB 980329, the observed red optical to near-IR afterglow spectrum (Palazzi *et al.* 1998) suggests a steep extinction curve. The best characterized (relatively) steep extinction law is for the Small Magellanic Cloud (SMC). We therefore adopt the SMC bar extinction curve from Weingartner & Draine (2001) , which is parameterized by the extinction level A_V in the rest frame of the host galaxy. Other extinction curves were used in model attempts and did not substantially change the results.

Depending on its luminosity, the host galaxy of the GRB may contribute a background level which dominates the total brightness at late times. This is observed as a flattening of the light curves, chiefly in the optical and IR. For GRB 980329, we include a constant term for the R, I, H and K to represent the host emission, and the values of these terms are fit by the model. The J-band only includes a single data point, so we interpolate the host term between the I and H fits. Evidence for host emission has also been observed at centimeter wavelengths (Berger, Kulkarni & Frail 2001), again deduced from late-time flattening of the lightcurve. The radiation at these wavelengths would most likely result from synchrotron and thermal bremsstrahlung in galaxies undergoing substantial star formation (Condon 1992). We include the possibility of centimeter host emission in our model, where we fit for the normalization at 1.43 GHz, and scale other bands as $\nu^{-0.8}$. In light of recent claimed detections of GRB hosts at submillimeter wavelengths (Hanlon *et al.* 2000; Berger, Kulkarni & Frail 2001; Frail *et al.* 2002; Berger *et al.* 2001b, 2002), we consider the possibility of a submillimeter host, and allow for such a component in the fit, with a modified blackbody as in Frail *et al.* (2001), parameterized by its flux at 350 GHz. This last host component was found not to be required for our best model.

4. Best-Fit Broadband Model

The afterglow model described in §3 was fit to the data summarized in Tables 1-3. In addition, we included all previously published data in the X-ray (In 't Zand *et al.* 1998), optical (Palazzi *et al.* 1998; Gorosabel *et al.* 1999; Reichart *et al.* 1999), and radio (Taylor *et al.* 1998) bands. We converted the X-ray measurements to flux values using a photon index of 2.4. We corrected the optical data for absorption in our Galaxy (Schlegel, Finkbeiner & Davis 1998) before converting to flux densities using the factors in Bessell (1979) for the optical and Bessell & Brett (1988) for the near-IR bands. To account for any cross-calibration uncertainty, we have added in quadrature 5% uncertainties to all the measured fluxes.

The model which best describes this broadband dataset is a collimated outflow expanding into a constant density medium. The best model parameters, derived from least-squares maximizing the fit probability, are summarized in Table 4 and Figs. 1-6. The χ^2 for the fit is 116.4 for 92 degrees of freedom. Although we derived fits for three representative redshifts ($z = 1, 2, 3$), the results of which are all shown in Table 4, we confine our detailed comments below to the $z = 2$ solution. This choice of representative redshifts was made based upon the range of likely z for this burst. Very high redshifts $z \gtrsim 5$ are not considered as they are not compatible with the underlying host's colors, as detailed in §4.1. A redshift $z < 1$ is considered implausible due to the lack of lines expected to be detected (if $z < 1$) in several spectra taken of the host. The host is visible at optical wavelengths, and thus not completely obscured, so it is quite unlikely that the prominent star-formation-related oxygen line [OII]λ3727 or the Hα line would not have been observable if the host is a faint galaxy at $z < 1$. Many of the basic conclusions do not depend on the redshift, or can be easily scaled given the information below. In §5 we discuss some of the limitations of our best fit, as well as some alternate models which also fit the data, but only with unphysical parameters.

In the best model for $z = 2$, the isotropic-equivalent fireball energy at the time when the fireball evolution becomes nearly adiabatic ($E_{\rm iso}(t_{\nu_c=\nu_m})$) is approximately 10^{54} ergs. The measured gamma-ray fluence for this GRB is $F_\gamma = 5.5 \times 10^{-5}$ erg cm^{-2} (In 't Zand *et al.* (1998)), so the isotropic gamma-ray energy is $E_{\rm iso}(\gamma) = 4\pi F_\gamma d_L^2 (1+z)^{-1} \simeq 6 \times 10^{53}$ erg. The large energy budgets inferred for both the shock $E_{\rm iso}(t_{\nu_c=\nu_m})$ and the emitted gamma-ray radiation $E_{\rm iso}(\gamma)$ derived assuming isotropy are greatly reduced in this model by the relatively large degree of collimation (jet opening angle of $\theta_{jet} \sim 2°$). A similar degree of collimation has been inferred previously in GRB afterglows: GRB 990510 has $\theta_{jet} = 3°$ (Harrison *et al.* 1999) and GRB 000911 has $\theta_{jet} = 2°$ (Price *et al.* 2002). For a two-sided jet this implies a total energy in the fireball shock of 8.3×10^{50} ergs, similar to the energy released in supernovae. Likewise, for $z = 2$ the geometry-corrected gamma-ray energy is reduced to 4.0×10^{50} erg, a value that is in good agreement with the mean of 5×10^{50} erg derived from a larger sample (Frail *et al.* 2001). We note the total energy is similar (5.4×10^{50}) for $z = 1$, and a factor of about three higher for $z = 3$.

The energy quoted in Table 4 is a lower limit on the true initial energy of the blastwave since it is derived at a time $t_{\nu_c=\nu_m}$=6.1 d, when the lowest energy electrons can cool within the dynamical timescale of the system. Observationally, this corresponds to the time when the cooling break ν_c crosses the spectral break which results from the low-energy cutoff in the input electron energy spectrum, ν_m. This criterion separates the two regimes of radiative losses; early times when radiant energy results in a decrease in the blastwave energy with time, and late times when the blast-wave evolution is adiabatic. For our best model, radiative losses are important, but not extreme even at early times, since the fraction of energy in radiating electrons is not dominant (ϵ_e=12%). We estimate that from the time the GRB ends ($\sim$ 10-100s post-trigger), to when the blastwave is nearly adiabatic, the energy drops by a factor of five. If we restrict the interval to begin when the first afterglow data were measured, ($t = 0.25$ d for the first data point to $t_{\nu_c=\nu_m}$), the energy drops by a factor of 1.6. From the time $t = t_{\nu_c=\nu_m}$ until late times the energy drops by only 15% .

The energy in the fireball derived from our model significantly exceeds the emitted gamma-ray energy, *i.e.,* $E_{\rm iso}(t_{\nu_c=\nu_m}) > E_{\rm iso}(\gamma)$. As discussed above, the initial fireball energy will be even larger if radiative losses are taken into account. This is the case for the majority of GRB afterglows with energies derived from model fits (see *e.g.* Panaitescu & Kumar (2001a)). In the fireball model, it is likely that the energy remaining in the shock during the afterglow exceeds that of the prompt gamma-ray emission of the GRB event itself; this will be the case for a radiative efficiency of $< 50\%$ during the GRB. The radiative efficiency of internal shocks driving the prompt GRB are expected to be $\sim 10\%$, not $\gg 50\%$, leaving most of the initial shock energy in the fireball (Guetta, Spada & Waxman 2001).

The ratio of the energy fraction in magnetic field, ϵ_B =17%, to that in the electrons, ϵ_e=12%, determines the relative importance of Comptonization. Compton scattering can contribute significantly to the total cooling rate if the ratio of electron to magnetic energy fractions is greater than unity (Sari & Esin 2001). In our best model for GRB 980329, this ratio is of order unity, so Comptonization does not dominate the electron cooling, but it is a non-negligible effect. Flux from Compton scattering can in fact be seen peaking in the X-rays in Figs. 4 and 6, largely as a result of the steep electron spectral index. For an electron energy spectral index of 2, with equal energies in each logarithmic frequency interval (the infinite-energy limit), the IC luminosity would be lower than the synchrotron luminosity at all frequencies, and no IC peak would be observable in the spectrum. The index of $p = 2.9$ derived for the best model puts less energy in each successive decade above the peak frequency. With a significant circumburst electron density providing a non-negligeable opacity to Compton scattering, the peak of the IC flux density, above the synchrotron peak, dominates the total flux near the X-rays.

The circumburst medium density derived from the model, $n = 20$ cm^{-3}, is comparable to that of GRB 000926 (Harrison *et al.* 2001) and that of several other bursts (Panaitescu & Kumar (2001a)). This relatively high density, in reference to an average galactic ISM, can be inferred from the measured value of the self-absorption break ν_a (Granot, Piran & Sari 1999), which is shown in Fig.6. The frequency ν_a depends upon other fundamental parameters besides the ambient density ($\nu_a \propto n^{3/5}\epsilon_e^{-1}\epsilon_B^{1/5}E_{iso}^{1/5}$), and in this particular case the high ν_a results from the relatively high density, combined with a moderate electron energy fraction. Models with low circumburst densities (*i.e.*, $n \ll 10$ cm^{-3}) cannot be fit to the data by adjusting the energy and electron fraction. Highly radiative models, with large electron energy fractions, can provide reasonable fits to the data, but the densities (depending on the redshift of the fit) vary from approximately the same as to an order of magnitude greater than those for the best model (see §5).

4.1. Host Galaxy

We infer the presence of measurable flux from the GRB host galaxy in the optical from the late-time flattening of the lightcurves (Fig. 3). In the final epoch of our optical observations the measured brightness of R=26.53±0.22 (see Table 1) is essentially entirely due to the host, and is only 1.5 mag fainter than the median R magnitude for known GRB host galaxies (Djorgovski *et al.* 2001). Our measured magnitude differs from the preliminary value of R=27.7±0.3 given by Holland *et al.* (2000). This discrepancy seems to be due to a mis-identification of the host in their HST images which they identify with a source 0.5″ southwest of the GRB position. Further work by that group (Jaunsen *et al.* 2002) has identified the host at a position consistent with that of Bloom *et al.* (2002), which established with improved astrometry the host whose R-band magnitude is given here. Bloom *et al.*'s (2002) measured offset for the GRB from the host center is only 37±48 mas, corresponding to a host-normalized offset of 0.215±0.291, placing GRB 980329 within the half light radius of its compact host. Our I band host flux values from Table 1 are in good agreement with

Jaunsen *et al.*'s (2002) late-time I band host measurement.

In Fig. 5 we plot the spectral energy distribution of the afterglow at 0.7 days after the burst along with the late-time measurements from Table 1, assumed to be due to the host galaxy. We corrected all points for extinction in our Galaxy. Palazzi *et al.* (1998) first noted the steep spectral slope between the R and I bands seen in the early time afterglow, and Fruchter (1999) suggested that this "dropout" of the R band could be produced by absorption from the Lyα forest if the redshift z of this burst was greater than five. This steep slope, however, is not reflected in the host spectrum. The afterglow at 0.7 days after the burst is significantly redder (R$-$I=2.7$\pm$0.4) than the host galaxy (R$-$I=0.2$\pm$0.3) itself (note that the quoted R$-$I above are corrected for Galactic extinction). From the absence of a strong $R-I$ break in the host spectrum, we can rule out a redshift of $z \gtrsim 5$ for GRB 980329.

Another result that emerges from the modeling is the presence of significant dust extinction in the host galaxy. Early attempts to model the optical data for this burst (Palazzi *et al.* 1998; Lamb, Castander & Reichart 1999) also found that the spectrum was substantially reddened by dust. Our fitted host $A_{\rm V}$ corresponds to hydrogen column density of $N_H \simeq 2 \times 10^{21}$ cm^{-2}, assuming a gas-to-dust ratio similar to that of the Milky Way (Predehl & Schmitt 1995; Reichart 2001). In't Zand *et al.* (1998) used the X-ray spectrum of the afterglow to derive a column density $N_H = 1.0 \pm 0.4 \times 10^{22}$ cm^{-2}, with a 99% confidence range of 1.3×10^{21}-1.5×10^{22} cm^{-2}, after subtracting a Galactic contribution of approximately $0.8{\times}10^{21}$cm^{-2} (Dickey & Lockman 1990). To translate this measured column into the restframe of the host galaxy requires multiplying by a factor $(1+z)^{8/3}$. For a redshift of 2, this exceeds the value derived from optical extinction. Such discrepancies have been noted before (Vreeswijk *et al.* 1999; Galama & Wijers 2001), and are taken as evidence of significant dust destruction in the circumburst medium out to a radius of order 10-20 pc (Waxman & Draine 2000; Fruchter, Krolik & Rhoads 2001; Reichart 2001). In the case of GRB 980329, however, the redshift is not known, and the uncertainties in the dust extinction law make it difficult to claim evidence for dust destruction.

There is a suggestion of a 1.43 GHz radio host in the data, with the model requiring a flat, positive component on average. Although the addition of this component improves the fit, the significance of a nonzero radio host parameter is only 3σ. If real, a radio host at $\simeq 25$ μJy would be about 1/3 the host flux density found for GRB 980703 (Berger, Kulkarni & Frail 2001). We note that the submillimeter data are in good agreement with the afterglow model (see Fig.2), and we do not require any host contribution in this band.

5. Alternate Models and Limitations

The best fit model given in §4, while not a unique interpretation of the data, is a self-consistent solution that derives reasonable values for the blastwave energy $E_{\rm iso}(t_{\nu_c=\nu_m})$, the opening angle θ_{jet}, the ambient density n and the parameters of the shock (p, ϵ_e, ϵ_B). A collimated outflow expanding into a constant density medium describes *all* the data well, addressing puzzling features described in previous attempts to fit this afterglow (Fruchter 1999; Lamb, Castander & Reichart 1999; Smith *et al.* 1999) without invoking a very high redshift or other additional components. The unusual features of this data set include the submillimeter excess, the very red $R-I$ afterglow colors and their relation to the host, and the observed decline of the peak flux density F_m with time (or equivalently with decreasing frequency ν_m, since ν_m decreases with time).

This last feature warrants further explanation, since it is an effect that can only result from a finite number of physical causes. The "peak flux cascade" can be readily seen in Figs. 1 and 2, where the peak flux density is 2.5 mJy at 350 GHz but declines to 1.5 mJy at 90 GHz and further falls to 0.35, 0.2 and <0.1 mJy at 8.46 GHz, 4.86 GHz, and 1.43 GHz, respectively. A fit to the data near maximum between 4.86 GHz and 350 GHz gives a power-law slope of 0.59±0.07. A similar behavior was also observed for the afterglow of GRB 970508 (Galama *et al.* 1998; Frail, Waxman & Kulkarni 2000). Within the context of the standard fireball model there are three ways to produce this behavior. First, if the flux evolution is observed after collimation of the ejecta becomes evident in the light curve decay (*i.e.*, post-jet), then $F_m \propto \nu_m^{1/2}$ (Sari, Piran & Halpern (1999)). For our best model, this is what produces the observed peak flux cascade. Alternately, a density gradient $n \propto r^{-2}$ in the surrounding medium (a stellar wind model) will give $F_m \propto \nu_m^{1/3}$ (Chevalier & Li 1999). Finally, radiative losses can produce a peak flux cascade. However, unless these are severe (namely most of the shock energy in electrons), the effect is quite weak. For example, for $\epsilon_e \simeq 0.1$, $F_m \propto \nu_m^{0.08}$, while for $\epsilon_e \simeq 1$, $F_m \propto \nu_m^{0.37}$ (Cohen, Piran & Sari 1998).

The other models we derived that fit the primary characteristics of the data all required unusual physical assumptions. For example, we found a solution with extreme radiative corrections (100% of the shock energy going into electrons) that could reproduce the observed peak flux cascade. Formally, this model fits the data better than the "best model" presented in the previous section, however, it reaches the unphysical edge of parameter space, and with extreme radiative losses our near-adiabatic treatment breaks down and cannot be fully trusted. The highly radiative model is isotropic, and for $z=2$, has the following parameters: $E_{\rm iso}(t_{\nu_c=\nu_m}) \simeq 2\times 10^{52}$ ergs, $n \simeq 20$ cm^{-3}, $p \simeq 2.02$, $\epsilon_B \simeq 0.17$, $\epsilon_e \to 1$, A(V) $\simeq 1.1$ and a centimeter host of $\simeq 17$ μJy at 1.43 GHz. In addition to the unphysical assumption about the electron energy partition, this model also has an electron spectral index approaching two, and hence a diverging total energy. This radiative model only accounts for $\approx 1/2$ of the 350 GHz flux, suggesting an underlying submillimeter host of $\simeq 0.7$ mJy (this component improves the fit at $\approx 3\,\sigma$ level). This submillimeter host flux level is just below the sensitivity limit of current instruments and would likely not be detectable at late times, if it indeed exists. We consider the collimated solution presented in §4 to be the best model as it is the best fit of the models with realistic parameters. This best model reproduces the flux cascade with a relatively narrow collimation angle (early jet-break). We note that the $p = 2.88$ we derive for the best $z = 2$ model is somewhat larger than found for other afterglows, which generally fall in the range $p = 2.2 - 2.4$. It is, however, physically reasonable, and we regard all the parameters associated with the best model as acceptable. The highly radiative solution is plotted along with the best model in the lightcurves presented in Figs. 1–4. The fit is visibly somewhat better, but at the cost of unphysical assumptions concerning the underlying parameters of the fireball.

The most serious limitation to modeling the afterglow of GRB 980329 is the lack of a good redshift estimate. Even a fairly comprehensive dataset such as this cannot constrain fundamental parameters without knowing the distance. This is because the synchrotron emission can be reproduced at different z simply by rescaling the physical parameters by appropriate powers of $(1 + z)$. Only "second order" effects such as host extinction, the IC component and radiative corrections do not directly re-scale with $(1 + z)$. In principle, we could include z as a free parameter in the model, and fit for the best value. In practice, however, the combination of the sparseness of the real dataset, and the uncertainties in the model prevent any unique redshift determination. This is evident from Table 4, where we show a good fit with reasonable physical parameters for all three redshifts.

The absence of a strong break in the host galaxy spectral colors (Fig. 5) allows us to place an upper limit on the host redshift. Spectral energy distribution (SED) fittings to host colors may place a stronger constraint (*e.g.* Castander & Lamb (1999), concerning the 970228 event), especially if the factor of $\sim$ four decline from K-band to I-band can be modelled by a Balmer break. Further HST imaging in optical bands might prove fruitful in this regard.

The absence of a redshift is responsible in part for the relatively large and uncertain estimate of the electron index p in our best model. The post-jet evolution of the optical light curves is determined by p (Sari, Piran & Halpern 1999). Unfortunately, this data is sparsely sampled at early times (Fig. 3), prior to when the host galaxy dominates the light. Likewise, the index p determines the shape of the synchrotron spectrum, and should therefore be derivable from the measurements. At optical wavelengths, however, there is a degeneracy between p and the dust extinction law — the latter of which can depend sensitively on z.

Lacking any knowledge about the extinction properties of dust in high redshift galaxies we adopted the SMC extinction law. Neither the X-ray spectral slope, nor the X-ray to optical flux ratio can break this degeneracy, since the contribution from inverse Compton scattering alters the X-ray flux normalization as well as the spectrum.

Finally, we note that both our best solution and the highly radiative solution fail to predict the early radio emission at 8.46 GHz ($t < 3$ d). This level of fluctuation is too great to be accounted for by the estimated ISS effects. Prompt, short-lived radio emission in excess of the normal afterglow component has been detected toward other GRBs (Kulkarni *et al.* 1999; Frail *et al.* 2000; Harrison *et al.* 2001). This is usually attributed to radiation from a reverse shock (Sari & Piran 1999), and we suggest that this may explain the bright early-time radio point for GRB 980329.

6. Conclusions

The new observations presented here, along with the data in the literature, form a complete collection of broadband measurements for the afterglow from the bright burst GRB 980329 beginning from early to late times. We have used these data together with a comprehensive fireball model to deduce fundamental physical parameters of the event (energy, geometry, density) and to measure the properties of the host galaxy.

The late-time optical/NIR data shows that the host is significantly bluer than the afterglow. Thus we reject the hypothesis that the very red afterglow colors were due to Lyman-α absorption in the intergalactic medium to a very high redshift source.

All of the afterglow's features can be explained over a wide range of z by a model in which the ejecta are collimated in a jet. Significant dust extinction is inferred within the host galaxy and a moderately high circumburst density $n \simeq 20$ cm^{-3} is required. Although this collimated model is not a unique solution to the data, it explains the red optical/NIR color and the cascade in the peak flux from submillimeter to centimeter wavelengths (see §5) without resorting to an extreme redshift $z \gtrsim 5$ or requiring additional complications in the host galaxy's properties. Models which invoke isotropic geometry require such complications, circumburst densities up to 10 times higher, as well as large, unphysical radiative corrections. Correcting the isotropic-equivalent gamma-ray energy release for the collimation, for $z = 2$ we obtain $E(\gamma) = E_{\rm iso}(\gamma)\theta^2/2 = 4.0 \times 10^{50}$ ergs. This value is typical of other events to date and is easily accounted for by current progenitor models.

RS acknowledges support from the Fairchild Foundation and from a NASA ATP grant.

JSB acknowledges a grant from the Hertz foundation. Research with the Owens Valley Radio Telescope, operated by Caltech, is supported by NSF grant AST96-13717

REFERENCES

Berger, E. *et al.* 2002, in preparation.

Berger, E. *et al.* 2001a, ApJ, 556, 556.

Berger, E. *et al.* 2001b, GCN notice 1182.

Berger, E., Kulkarni, S. R., and Frail, D. A. 2001, ApJ, 560, 652.

Berger, E. *et al.* 2000, ApJ, 545, 56.

Bessell, M. S. 1979, PASP, 91, 589.

Bessell, M. S., and Brett, J. M. 1988, PASP, 100, 1134.

Bloom, J. S., Frail, D. A., and Sari, R. 2001, AJ, 121, 2879.

Bloom, J. S., Kulkarni, S. R., and Djorgovski, S. G. 2002, AJ, 123, 1111.

Castander, F. J. and Lamb, D. Q. 1999, ApJ, 523, 593.

Chevalier, R. A. and Li, Z.-Y. 1999, ApJ, 520, L29.

Cohen, E., Piran, T., and Sari, R. 1998, ApJ, 509, 717.

Condon, J. J. 1992, Ann. Rev. Astr. Ap., 30, 575.

Coulson, I. M. 2000, (http://www.jach.hawaii.edu/JACpublic/JCMT/Continuum-observing/SCUBA/astronomy/calibration/gains.html).

Dickey, J. M. and Lockman, F. J. 1990, Ann. Rev. Astr. Ap., 28, 215.

Djorgovski, S. G. *et al.* 1998, GCN notice 41.

Djorgovski, S. *et al.* 2001, To appear in: Proc. IX Marcel Grossmann Meeting, eds. V. Gurzadyan, R. Jantzen, and R. Ruffini, Singapore: World Scientific, in press; astro-ph/0106574.

Djorgovski, S. G., Frail, D. A., Kulkarni, S. R., Bloom, J. S., Odewahn, S. C., and Diercks, A. 2001, ApJ, 562, 654.

Frail, D. A. *et al.* 2000, ApJ, 538, L129.

Frail, D. A. *et al.* 2002, ApJ, 565, 829.

Frail, D. A., Kulkarni, S. R., Nicastro, S. R., Feroci, M., and Taylor, G. B. 1997, Nature, 389, 261.

Frail, D. A. *et al.* 2001, ApJ, 562, L55.

Frail, D. A., Waxman, E., and Kulkarni, S. R. 2000, ApJ, 537, 191.

Fruchter, A., Krolik, J. H., and Rhoads, J. E. 2001, ApJ, 563, 597.

Fruchter, A. S. 1999, ApJ, 512, L1.

Galama, T. J. and Wijers, R. A. M. J. 2001, ApJ, 549, L209.

Galama, T. J. *et al.* 1998, ApJ, 500, L101.

Goodman, J. 1997, New Astr., 2(5), 449.

Gorosabel, J., Castro-Tirado, A. J., Pedrosa, A., Zapatero-Osorio, M. R., Fernades, A. J. L., Feroci, M., Costa, E., and Frontera, F. 1999, A&A, 347, L31.

Granot, J., Piran, T., and Sari, R. 1999, ApJ, 527, 236.

Guetta, D., Spada, M., and Waxman, E. 2001, ApJ, 557, 399.

Hanlon, L. *et al.* 2000, A&A, 359, 941.

Harrison, F. A. *et al.* 1999, ApJ, 523, L121.

Harrison, F. A. *et al.* 2001, ApJ, 559, 123.

Holland , S. *et al.* 2000, GCN notice 778.

In 't Zand, J. J. M. *et al.* 1998, ApJ, 505, L119.

Jaunsen, A. O. *et al.* A&A, submitted; astro-ph/0204278.

Jenness, T. and Lightfoot, J. F. 1998, in ASP Conf. Ser. 145: Astronomical Data Analysis Software and Systems VII, volume 7, 216.

Jenness, T., Lightfoot, J. F., and Holland, W. S. 1998, Proc. S.P.I.E., 3357, 548.

Klose, S. 1998, GCN notice 43.

Klose, S. *et al.* 2000, ApJ, 545, 271.

Kulkarni, S. R. *et al.* 1999, ApJ, 522, L97.

Lamb, D. Q., Castander, F. J., and Reichart, D. E. 1999, A&AS, 138, 479.

Larkin, J., Ghez, A., Kulkarni, S., Djorgovski, S., Frail, D., and Taylor, G. 1998a, GCN notice 44.

Larkin, J., Ghez, A., Kulkarni, S., Djorgovski, S., Frail, D., and Taylor, G. 1998b, GCN notice 51.

Matthews, K. and Soifer, B. T. 1994, in ASSL Vol. 190: Astronomy with Arrays, The Next Generation, 239.

Oke, J. B. *et al.* 1995, PASP, 107, 375.

Palazzi, E. *et al.* 1998, A&A, 336, L95.

Panaitescu, A. and Kumar, P. 2001a, ApJ, 560, L49.

Panaitescu, A. and Kumar, P. 2001b, ApJ, 554, 667.

Persson, S. E., Murphy, D. C., Krzeminski, W., Roth, M., and Rieke, M. J. 1998, AJ, 116, 2475.

Piran, T. 1999, Phys. Rep., 314, 575.

Predehl, P. and Schmitt, J. H. M. M. 1995, A&A, 293, 889.

Price *et al.* 2002, ApJ in press; astro-ph/0110315.

Reichart, D. E. 2001, ApJ, 553, 235.

Reichart, D. E. 2001, ApJ, submitted; astro-ph/0107546.

Reichart, D. E. *et al.* 1999, ApJ, 517, 692.

Sari, R. and Esin, A. A. 2001, ApJ, 548, 787.

Sari, R. and Piran, T. 1999, ApJ, 517, L109.

Sari, R., Piran, T., and Halpern, J. P. 1999, ApJ, 519, L17.

Sari, R., Piran, T., and Narayan, R. 1998, ApJ, 497, L17.

Schlegel, D. J., Finkbeiner, D. P., and Davis, M. 1998, ApJ, 500, 525.

Sheinis, A. I., Miller, J. S., Bolte, M., and Sutin, B. M. 2000, in Proc. SPIE Vol. 4008, p. 522-533, Optical and IR Telescope Instrumentation and Detectors, Masanori Iye; Alan F. Moorwood; Eds., volume 4008, 522.

Smith, I. A. *et al.* 1999, A&A, 347, 92.

Sokolov, V. V. *et al.* 2001, A&A, 372, 438.

Stephens, A. W., Frogel, J. A., Ortolani, S., Davies, R., Jablonka, P., Renzini, A., and Rich, R. M. 2000, AJ, 119, 419.

Taylor, G. B. *et al.* 1998, ApJ, 502, L115.

Vreeswijk, P. M. *et al.* 1999, ApJ, 523, 171.

Walker, M. A. 1998, MNRAS, 294, 307.

Waxman, E. and Draine, B. T. 2000, ApJ, 537, 796.

Weingartner, J. C. and Draine, B. T. 2001, ApJ, 548, 296.

Wijers, R. A. M. J. and Galama, T. J. 1999, ApJ, 523, 177.

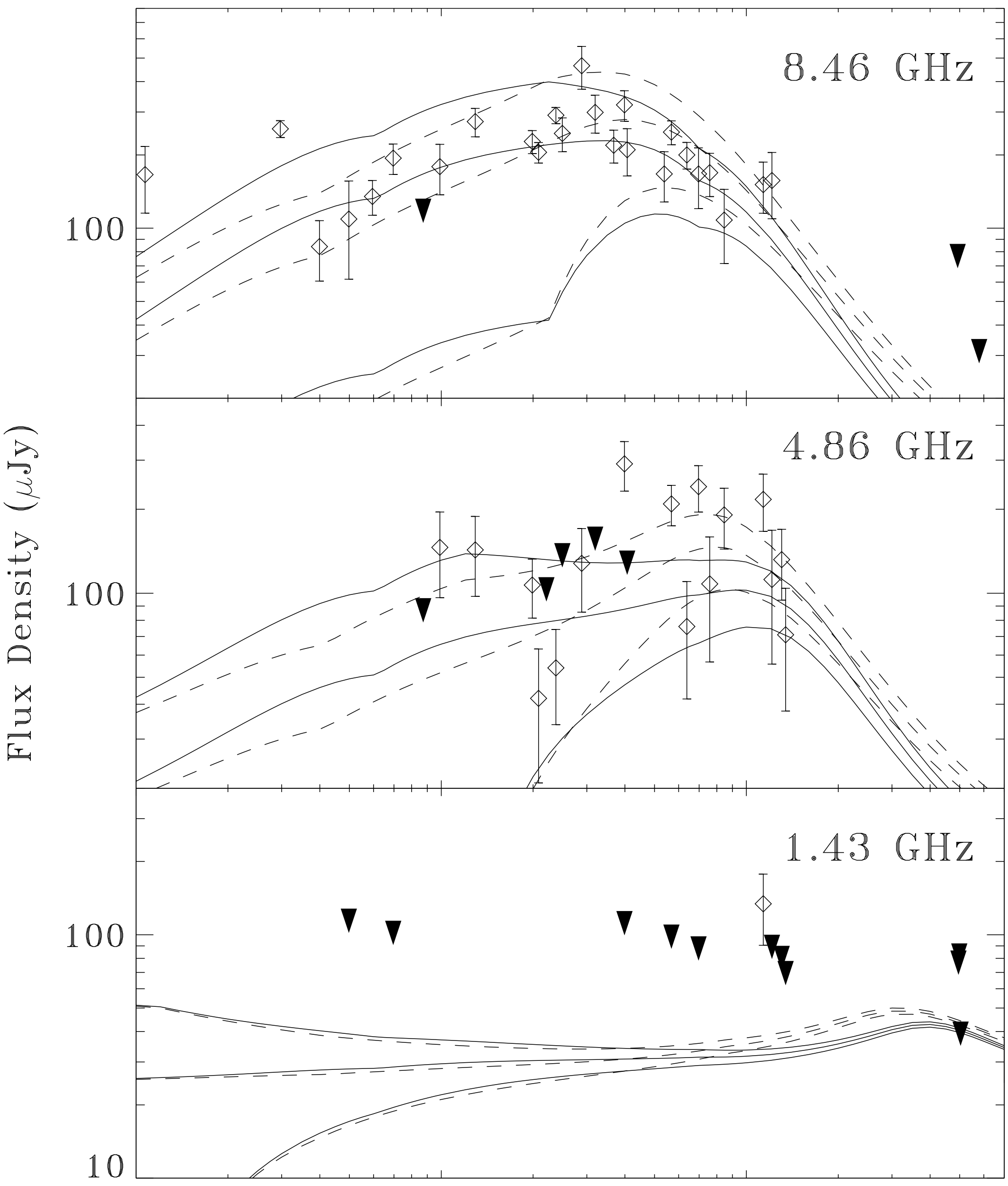

Fig. 1.— Radio lightcurves of the GRB 980329 afterglow. Both the best model and the extreme radiative solution, described in §5 are plotted. The light curves of the "best" model (the best physical model; see §4 and 5 for details) are solid; the radiative solution's are dashed. The model lightcurves are plotted with their calculated 1-σ scintillation envelopes above and below. Data that are not at least detected at the 2-σ level are presented as 2-σ upper limits (max(flux density, 0) + 2 $\times$ rms noise; black triangles). The 1.43 GHz data is only significant as a whole. Note that the 8.46 GHz data at $\leq$ 3 days, which was not included in the fits, is significantly in excess of both models.

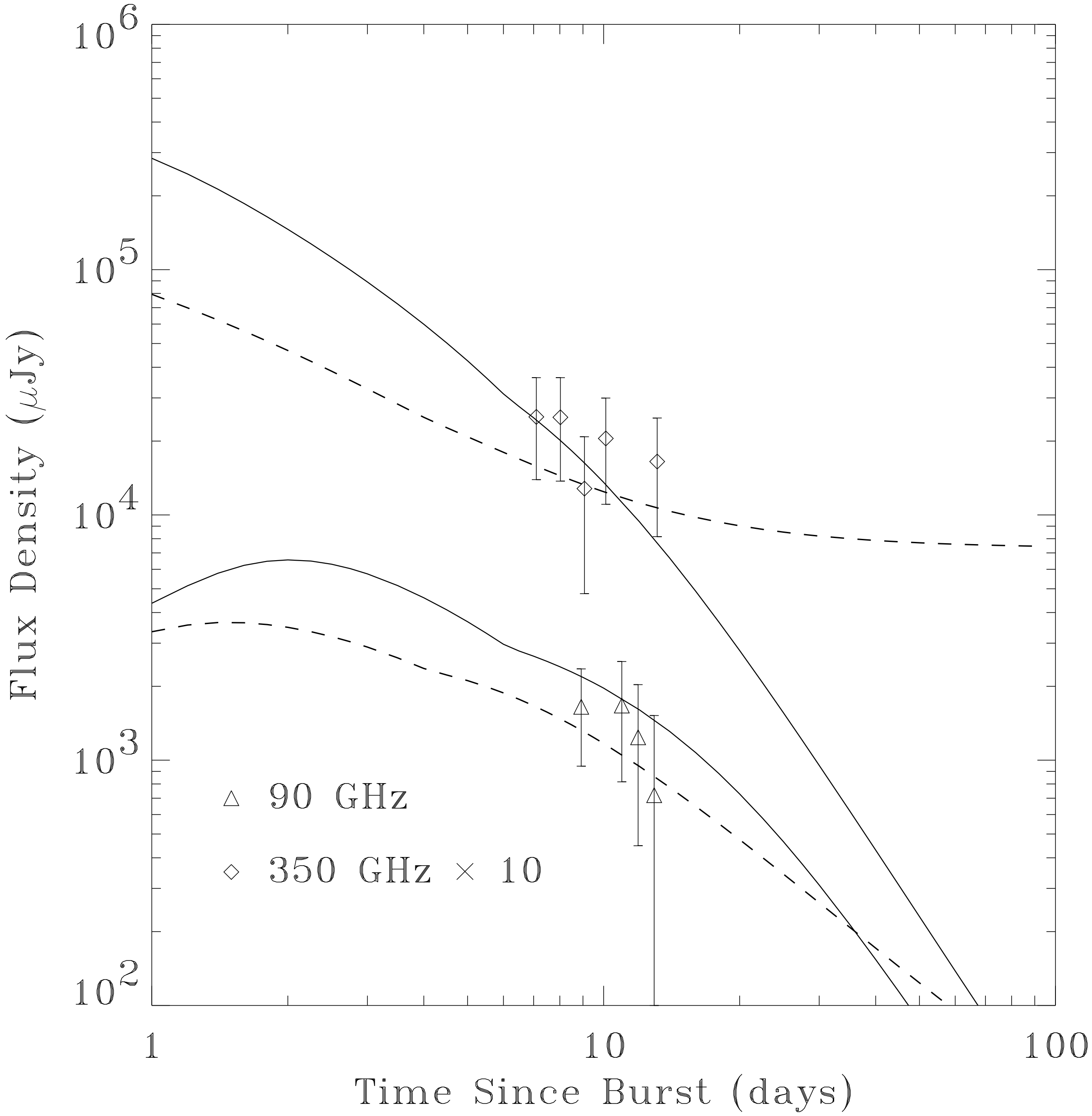

Fig. 2.— Millimeter and submillimeter lightcurves of the GRB 980329 afterglow; the 350 GHz data and model are multiplied by 10 for clarity. The "best" model (the best physical model; see §4 and 5 for details) is shown with solid lightcurves; the radiative solution (§5) with dashed ones. The best model fits the reanalyzed data without the need to include a submillimeter host component. The radiative solution is plotted with the submillimeter host component, required to account for $\sim 1/2$ of the 350 GHz flux. See the text for model details.

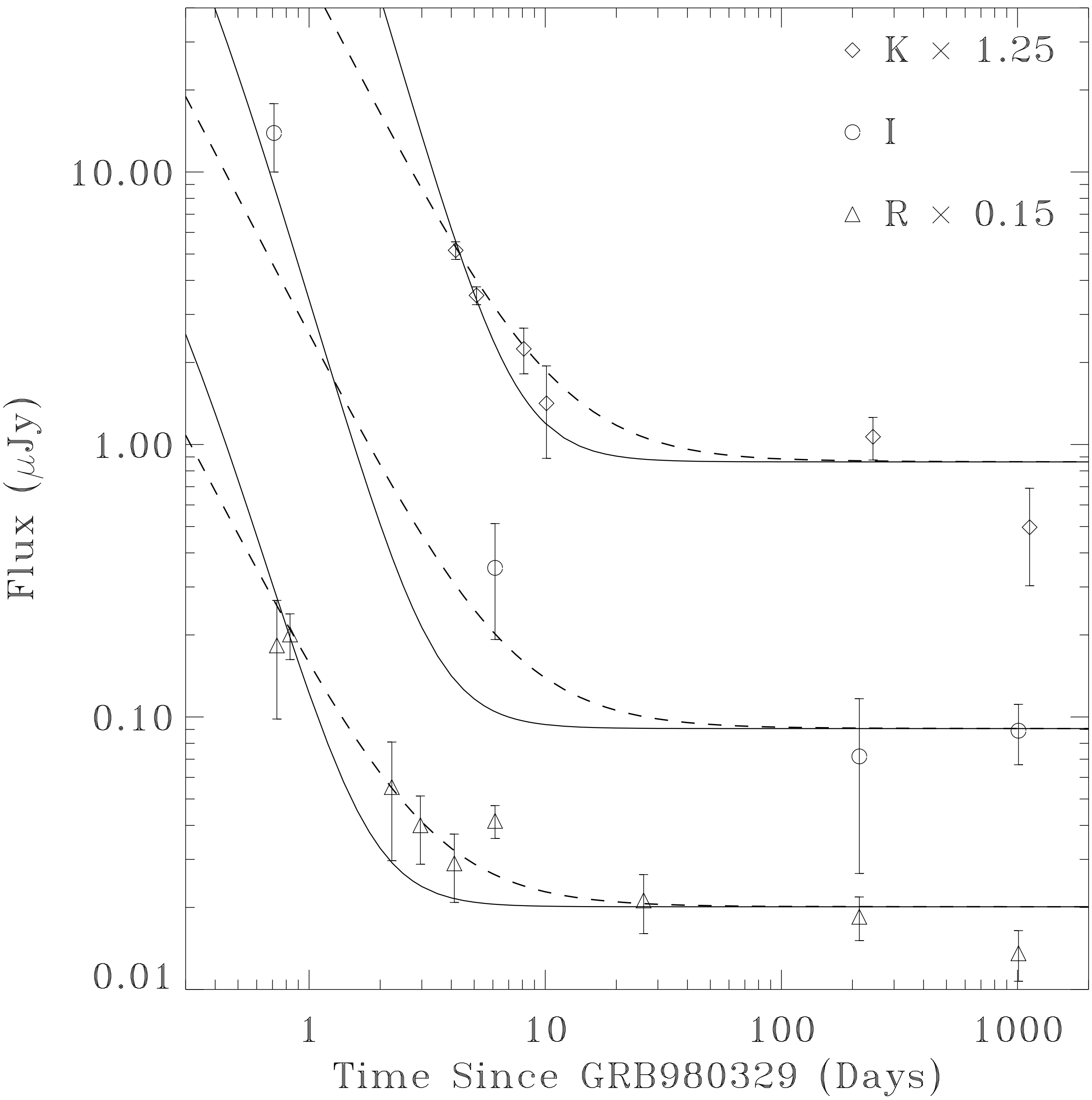

Fig. 3.— Optical lightcurves of the GRB 980329 afterglow at R, I and K bands. The "best" model (the best physical model; see §4 and 5 for details) is shown with solid lightcurves; the extreme radiative solution (§5) with dashed ones. The data are corrected for Galactic (but not host) extinction. The late-time host fluxes can be clearly seen.

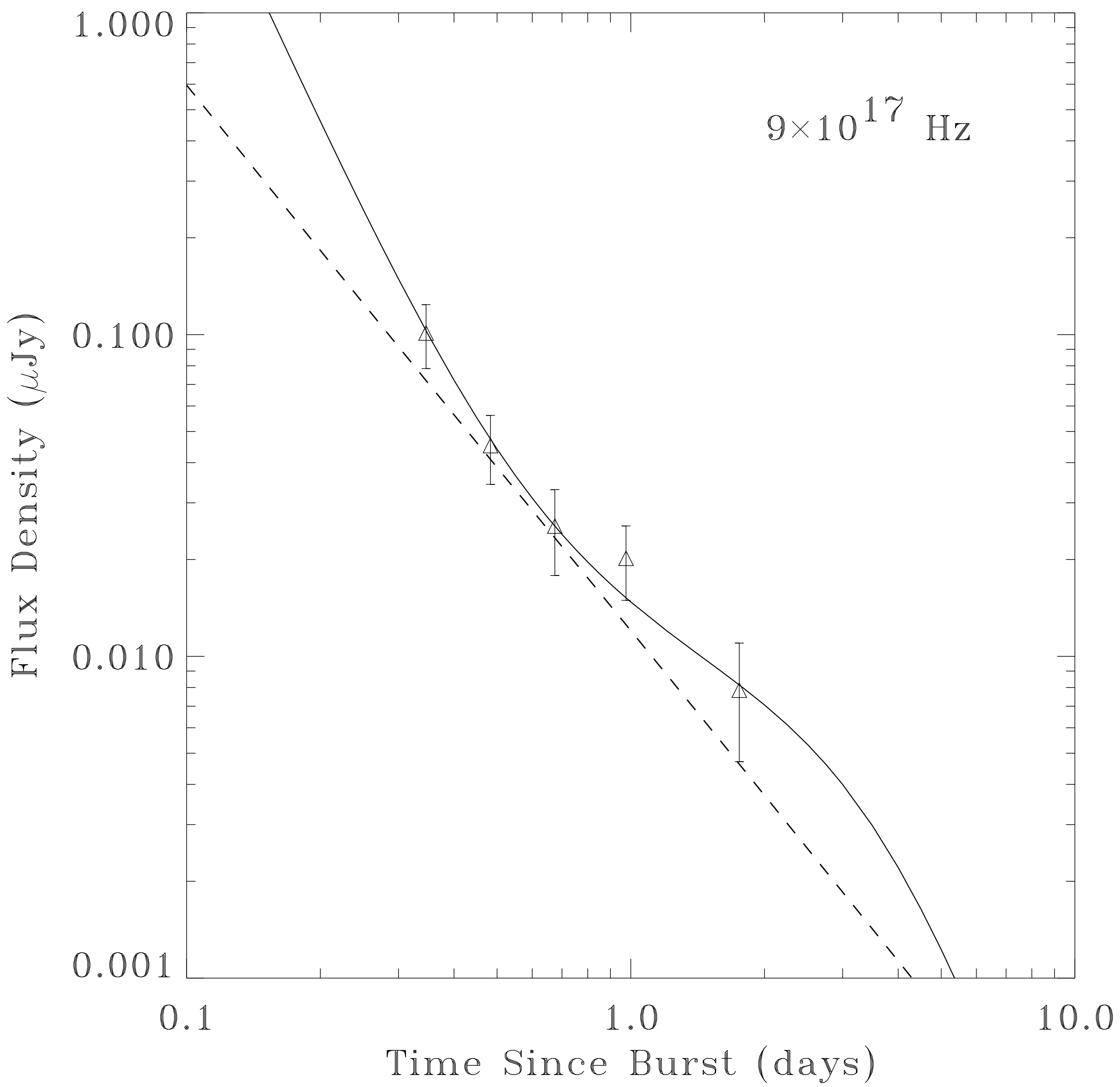

Fig. 4.— The X-ray lightcurve of the GRB 980329 afterglow, with both models. The "best" model (the best physical model; see §4 and 5 for details) is shown with solid lightcurves; the extreme radiative solution (§5) with dashed ones (see text for details). The curvature seen in the best model after 2 days is the signature of a significant inverse Compton contribution to the X-ray afterglow flux at that time.

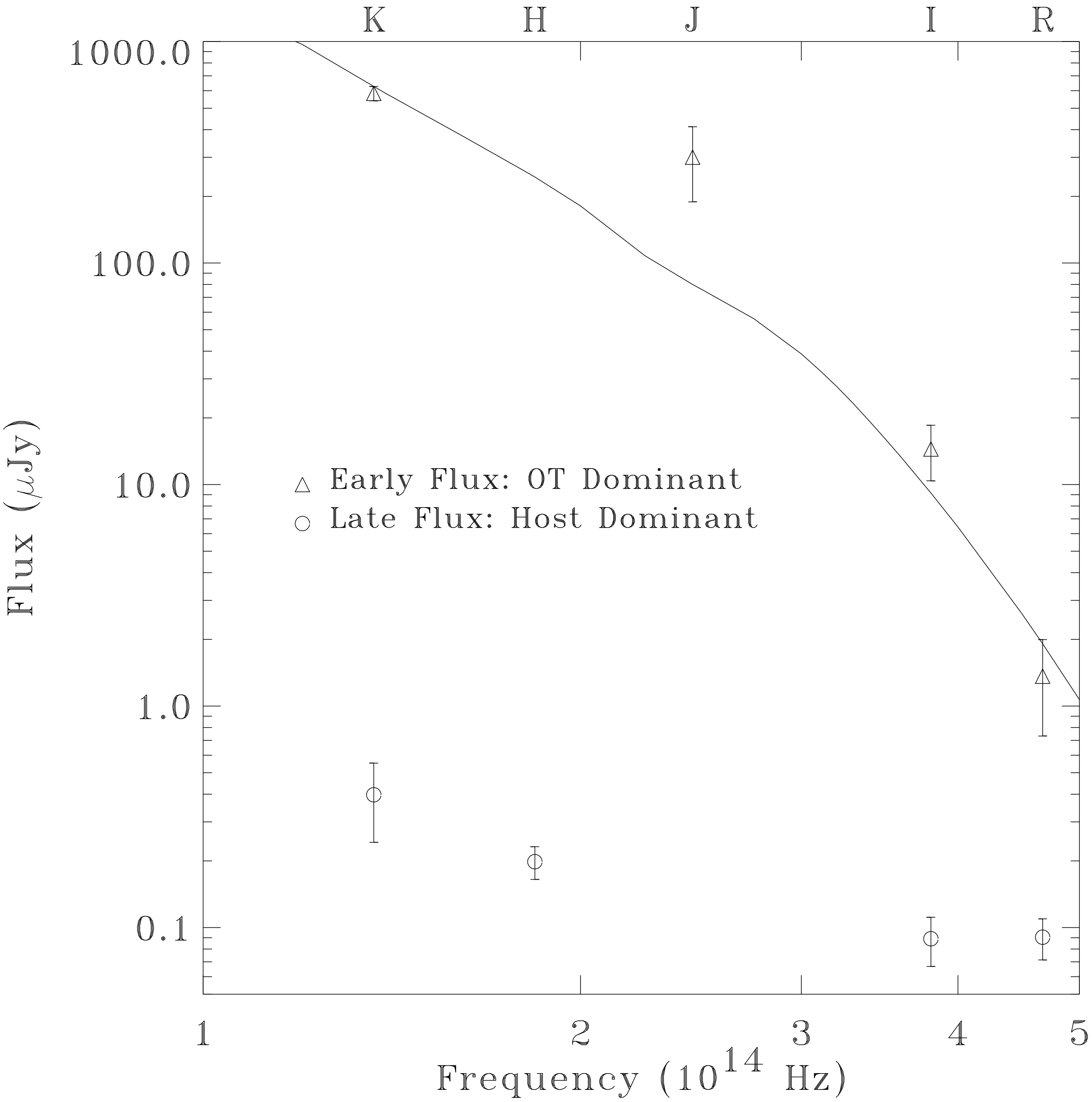

Fig. 5.— Comparison of afterglow and underlying host optical flux densities. The data are corrected for Galactic (but not host) extinction. The first available data points (open triangles) in R, I, J, and K bands (at 0.73, 0.71, 8.1 and 4.2 days post-burst respectively) were each scaled to 0.7 days using our best afterglow model, which is overplotted. The afterglow flux dominates these points and the spectral steepness from I to R is clearly seen. (Note that the J band point, being extrapolated from a time when the host flux was beginning to become important, is a less reliable afterglow flux indicator.) The late time measurements (open circles) at R, I, H, and K bands are also plotted to show the host spectrum. The host spectrum does not show the steep spectral slope between the I and R bands, as expected if GRB 980329 was at $z \gtrsim 5$ (see text for details).

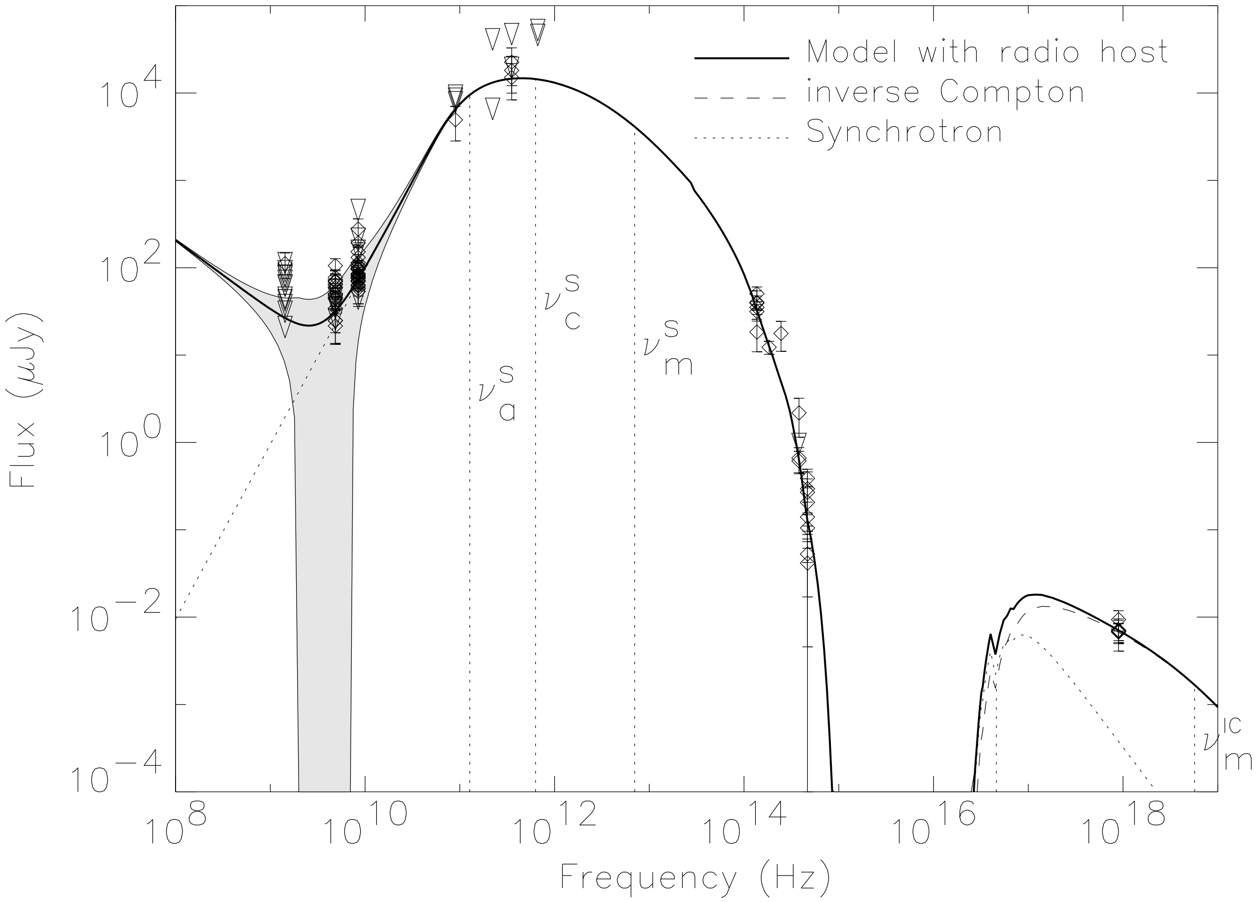

Fig. 6.— All of the data, scaled to day 2 post-burst, and plotted on our model's day 2 spectrum. The spectrum's inverse Compton and synchrotron flux components are decomposed from the total. The grey shaded region represents the estimated flux uncertainty in the model of the observed spectrum at this time, due to interstellar scintillation. The high self-absorption frequency and predominance of the Comptonized flux at X-ray frequencies can be clearly seen.

Table 1. Optical/NIR Observations of GRB 980329

Epoch (UT)	Telescope	Inst.	Band	Mag.
1998 Apr. 04.29	Keck	LRIS	R	25.31 ± 0.14
1998 Apr. 24.25	Keck	LRIS	R	$26.04^{+0.30}_{-0.23}$
1998 Nov. 29	Keck	LRIS	R	26.19 ± 0.19
2001 Jan. 01.32	Keck	ESI	R	$26.53^{+0.25}_{-0.20}$
1998 Apr. 04.29	Keck	LRIS	I	$24.79^{+0.65}_{-0.40}$
1998 Nov. 29	Keck	LRIS	I	$26.52^{+1.07}_{-0.53}$
2001 Jan. 01.32	Keck	ESI	I	$26.28^{+0.31}_{-0.24}$
1998 Oct. 16	HST	NICMOS	H	$24.32^{+0.19}_{-0.16}$
1998 Apr 02.33	Keck	NIRC	K	20.50 ± 0.06
1998 Apr 03.27	Keck	NIRC	K	20.91 ± 0.06
1998 Nov 28.49	Keck	NIRC	K	22.21 ± 0.19
2001 Apr 27.25	Keck	NIRC	K	$23.04^{+0.53}_{-0.36}$

Table 2. VLA Observations of GRB 980329

Epoch (UT)	Frequency (GHz)	Flux Density (μJy)
1998 May 04.92	8.46	219±32
1998 May 08.01	8.46	321±43
1998 May 08.84	8.46	210±45
1998 May 21.97	8.46	167±38
1998 May 24.96	8.46	248±25
1998 May 31.98	8.46	200±23
1998 Jun. 06.84	8.46	167±46
1998 Jun. 12.98	8.46	169±33
1998 Jun. 21.77	8.46	108±36
1998 Jul. 20.70	8.46	151±35
1998 Jul. 28.43	8.46	157±47
1999 Aug. 03.60	8.46	40±23
1999 Oct. 29.43	8.46	13±11
2000 Sep. 01.40	8.46	−8.0±14
1998 May 08.01	4.86	291±57
1998 May 08.84	4.86	60±41
1998 May 24.96	4.86	209±33
1998 May 31.98	4.86	76±34
1998 Jun. 06.84	4.86	241±44
1998 Jun. 12.98	4.86	108±51
1998 Jun. 21.77	4.86	191±46
1998 Jul. 20.70	4.86	217±49
1998 Jul. 28.43	4.86	112±56
1998 Aug. 06.68	4.86	132±37
1998 Aug. 10.58	4.86	71±33
1998 May 08.01	1.43	47±39
1998 May 24.96	1.43	42±34
1998 Jun. 06.84	1.43	0.5±49
1998 Jul. 20.70	1.43	134±43
1998 Jul. 28.43	1.43	16±42
1998 Aug. 06.68	1.43	−39±45
1998 Aug. 10.58	1.43	−17±39
1999 Aug. 06.68	1.43	36±25
1999 Aug. 09.63	1.43	40±26
1999 Aug. 14.65	1.43	−1.7±22

Table 3. Millimeter Observations of GRB 980329

Epoch (UT)	Frequency (GHz)	Flux Density[a] (mJy)
1998 Apr. 5.25	650	-9.9 ± 9.3
1998 Apr. 6.18	650	-11.8 ± 8.9
1998 Apr. 7.22	650	0.1 ± 7.5
1998 Apr. 8.27	650	0.4 ± 8.5
1998 Apr. 11.30	650	-1.1 ± 5.1
1998 Apr. 5.25	350	2.51 ± 1.11
1998 Apr. 6.18	350	2.50 ± 1.12
1998 Apr. 7.22	350	1.28 ± 0.80
1998 Apr. 8.27	350	2.05 ± 0.94
1998 Apr. 11.30	350	1.65 ± 0.83
1998 Apr. 7.30	220	3.69 ± 2.18
1998 Apr. 8.16	220	-0.96 ± 1.04
1998 Dec. 13.91	100.0	0.04 ± 0.70
2001 Nov. 26.48	99.5	0.54 ± 0.50

[a]Due to our recalibration of the data, the submillimeter fluxes presented here are in disagreement with Smith *et al.* (1999)'s values from the same observations, and in good agreement with the afterglow model with no host excess (see Fig.2).

Table 4. Fit parameters for assumed $z = 1, 2, 3$

Parameter	z=1	z=2	z=3
χ^2 for 105 data pts	113.1	116.4	119.4
$t_{\rm jet}$ (days)	0.21	0.12	0.29
$t_{\rm nonrel.}$ (days)	35	70	96
$t_{\nu_{\rm c}=\nu_{\rm m}}$ (days)	2.4	6.1	10.0
$E_{\rm iso}(t_{\nu_c=\nu_m})(10^{52}$ erg)[a]	15	126	107
$n(cm^{-3})$	20	20	29
p	2.55	2.88	3.06
ϵ_e (fraction of E)	0.08	0.12	0.14
ϵ_B (fraction of E)	0.27	0.17	0.08
$\theta_{jet}(rad)$	0.081	0.036	0.049
host A(V)	2.8	1.9	1.4
host R (μJy)	0.13	0.13	0.13
host I (μJy)	0.090	0.091	0.090
host H (μJy)	0.20	0.20	0.20
host K (μJy)	0.68	0.69	0.70
host 1.4 GHz (μJy)	19	25	26
$E_{\rm iso}(\gamma)$[b](10^{53} erg)	1.5±0.2	5.1±0.6	9.5±1.1
$E(\gamma)$ (10^{50} erg)[c]	5.0±0.6	3.3±0.4	11±1

[a]Isotropic equivalent blastwave energy (not corrected for collimation)

[b]Isotropic-equivalent energy emitted in the gamma-rays by the GRB, if it occurred at this redshift, calculated by the method of Bloom et al. (2001)

[c]The isotropic-equivalent energies given above, corrected assuming the jet angles (without uncertainty) presented above